

Modeling Galaxies in the Early Universe with Supernova Dust Attenuation

JED MCKINNEY,^{1,*} OLIVIA R. COOPER,^{1,†} CAITLIN M. CASEY,² JULIAN B. MUÑOZ,¹ HOLLIS AKINS,^{1,‡}
ERINI LAMBRIDES,^{3,‡} AND ARIANNA S. LONG⁴

¹*Department of Astronomy, The University of Texas at Austin, Austin, TX, USA*

²*Department of Physics, University of California Santa Barbara, Santa Barbara, CA, USA*

³*NASA-Goddard Space Flight Center, Code 662, Greenbelt, MD, 20771, USA*

⁴*Department of Astronomy, University of Washington, Seattle, WA, USA*

ABSTRACT

Supernova may be the dominant channel by which dust grains accumulate in galaxies during the first Gyr of cosmic time as formation channels important for lower redshift galaxies, e.g., AGB stars and grain growth, may not have had sufficient time to take over. Supernovae (SNe) produce fewer small grains, leading to a flatter attenuation law. In this work, we fit observations of 138 spectroscopically confirmed $z > 6$ galaxies adopting standard spectral energy distribution modeling assumptions and compare standard attenuation law prescriptions to that of supernova-produced dust alone. Compared to SMC dust, SNe attenuation yields up to 0.5 mag higher A_V , and 0.4 dex larger stellar masses. SNe dust attenuation also finds better fits to the rest-frame UV photometry with lower χ^2_{UV} . This allows the observed UV luminosities taken from the models to be fainter by 0.2 dex on average. The systematically fainter observed UV luminosities for fixed observed photometry could help resolve current tension between the ionizing photon production implied by *JWST* observations and the redshift evolution of the neutral hydrogen fraction. Given these systematic effects and the physical constraint of cosmic time itself, pure supernova dust attenuation laws should be a standard consideration in fitting to the spectral energy distributions of $z > 6$ galaxies.

1. INTRODUCTION

The presence of dust grains in galaxies at very early times can significantly change inferred properties like total stellar mass and UV luminosity, key metrics for assessing the evolutionary pathways by which galaxy evolution begins. Historically, dust is thought to be subdominant in galaxies until $z \lesssim 3 - 4$ (e.g., Zavala et al. 2021) at which point galaxies have had enough time to grow dust reservoirs via Asymptotic Giant Branch (AGB) stars undergoing dust-enriched mass loss. However, direct observations of dust in emission exists up to $z = 8.3$ (Tamura et al. 2019) while indirect evidence from carbon enrichment, Balmer decrements, and UV continuum slopes extend to $z = 12$ (Bunker et al. 2023; Zavala et al. 2024; Langeroodi et al. 2024). Recently, Schneider & Maiolino (2024) review theoretical mechanisms that might produce dust at such early cosmic times, demonstrating that core collapse Supernovae (SNe) are the most likely grain-formation channel in the

first Gyr given the relevant timescales and dust yields (see also Todini & Ferrara 2001; Nozawa et al. 2003). By $z > 6$ the age of the Universe is < 1 Gyr which is prohibitively close to the 0.5 Gyr needed for any low-mass ($\lesssim 2M_\odot$) stars to evolve off the main-sequence. Other plausible mechanisms include dust formation in winds driven by active galactic nuclei (Sarangi et al. 2019), or ambient grain growth in the cold interstellar medium (Draine & Salpeter 1979; Draine 2009; Popping et al. 2017) — two channels with highly uncertain yields and end state grain properties, especially in exotic systems like the first galaxies.

What is to be done considering the effects of dust on observations of very high-redshift galaxies? One option is to assume that the effects of dust attenuation are extremely low (Ferrara et al. 2023; Ferrara 2024; Ferrara et al. 2024a,b; Ziparo et al. 2023; Fiore et al. 2023). This is a reasonable assumption, but one that should be made explicitly clear in observational works handling properties highly sensitive to the presence of dust like total stellar mass. Even among the most obscured galaxies in the Universe, dust only constitutes $< 1\%$ of the ISM by mass (Scoville et al. 2017). In other words, a little bit of dust goes a long way in shaping the observed, and

* NASA Hubble Fellow

† NSF Graduate Research Fellow

‡ NPP Fellow

intrinsic, properties of galaxies. Moreover, observations of very high-redshift galaxies typically do not probe the rest-frame optical so any dust constraint relies on extrapolating from the rest-frame UV which exacerbates any uncertainty arising from dust assumptions.

Should our assumptions about $z > 6 - 8$ dust change, photometry and spectra should be corrected using our knowledge of dust attenuation laws and dust formation pathways. This is now largely being done by applying well-understood attenuation laws tied to local Universe observations (e.g., Topping et al. 2024). This is well-motivated by the fact that SMC attenuation laws (Gordon et al. 2003) have been shown to work well for low metallicity, high-redshift galaxies (Reddy et al. 2015), and also because Milky Way laws (Cardelli et al. 1989) harbor the broad 2175Å feature that has now been spectroscopically confirmed at $z = 6.33$ (Witstok et al. 2023). None of these attenuation laws are explicitly representative of the dust grains expected to arise purely from SNe which could be producing most of the dust. Recent works such as Markov et al. (2023, 2024) and Fisher et al. (2025) are flexibly modeling the attenuation law shape directly, which is a promising approach for incorporating dust attenuation uncertainties into modeling results, and also for inferring trends in the underlying shape. There is growing evidence for shallower attenuation at $z > 6$ which could arise from an abundance of SNe dust (e.g., Ferrara et al. 2022; Markov et al. 2023, 2024; Fisher et al. 2025).

The dust grain size distribution is one of the most important factors dictating the shape of an attenuation law (Salim & Narayanan 2020), and grain size yields from SNe are not representative of those found in the SMC, or the Milky Way on-average. SNe dust is generally characterized by a deficit in the small grains leading to gray UV attenuation (e.g., Nozawa et al. 2003; Hirashita et al. 2005). In this letter, we argue that the first approach to accounting for dust in galaxies at high-redshift ($z \gtrsim 6 - 8$) should be to assume a pure SNe-derived attenuation law. This assumption has precedent among highly obscured $z \sim 1$ galaxies (Kawara et al. 2011; Shimizu et al. 2011), quasars at the tail end of the epoch of reionization (Hirashita et al. 2005; Bianchi & Schneider 2007), and is consistent with the findings of Markov et al. (2023, 2024), Langeroodi et al. (2024), and Fisher et al. (2025) at $z > 6$. In Section 2 we compare attenuation laws and discuss the SNe law that we adopt in this analysis. Section 3 presents the sample of galaxies that we fit under the SNe dust assumption with spectral energy distribution modeling as described in Section 4. We summarize our results in Section 5 and discuss their implications in Section 6. Throughout this work we as-

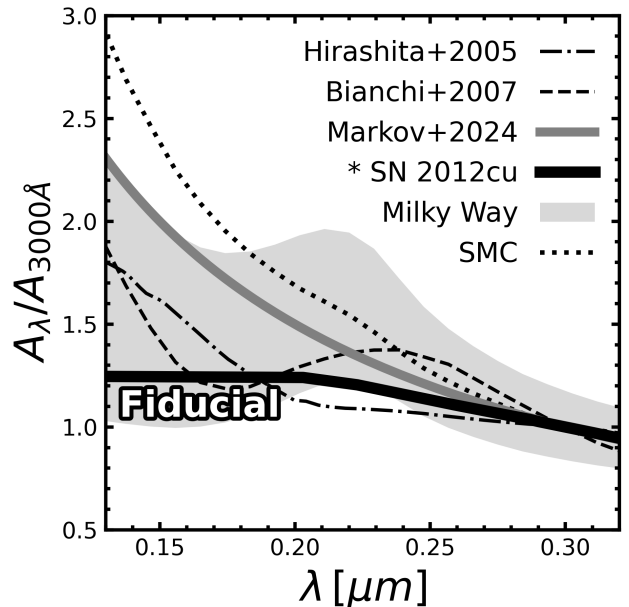


Figure 1. UV attenuation laws normalized at 3000Å for various dust models and observations. Milky Way attenuation laws span the range shaded in gray, and the SMC law, often taken as standard for very high-redshift galaxies, is shown with the dotted line. The thick gray line shows the inferred attenuation law from Markov et al. (2024) who fit to JWST spectra of galaxies with $6.3 < z < 11.5$. In solid black we show the empirical attenuation law measured by Gao et al. (2020) for SNe 2012cu, which we adopt as our fiducial SNe dust law. This empirical attenuation law is comparable to the theoretical models of SNe dust from Hirashita et al. (2005) and Bianchi & Schneider (2007), although the models tend to have steeper UV slopes. In general, attenuation by SNe dust in the UV is flatter than the SMC law due to the absence of very small ($a \approx 0.01 \mu\text{m}$) dust grains.

sume a Λ CDM cosmology with $H_0 = 70 \text{ km s}^{-1} \text{ Mpc}^{-1}$, $\Omega_m = 0.3$, $\Omega_\Lambda = 0.7$, a Kroupa initial mass function (IMF, Kroupa 2001), and the AB magnitude system (Oke 1974).

2. THE SUPERNOVA DUST ATTENUATION LAW

We begin by describing the attenuation law A_λ properties of SNe dust which has been constrained observationally and also modeled theoretically. Gao et al. (2020) derive A_λ from observations of the red type Ia SN 2012cu. Their derived attenuation law is notably flat into the UV and does not exhibit a pronounced 2175Å bump. Hirashita et al. (2005) investigate the extinction curves arising from Pop III into either SNe Type II or pair instability SNe (PISNe) both based on the Pop III models and elemental yields of Nozawa et al. (2003). For larger SNe II progenitor masses ($\approx 20 M_\odot$) and PISNe both with well-mixed helium cores, the Pop

III models predict very steep extinction in the UV tied to a high abundance small grains. Less massive SNe II progenitors ($\approx 13M_{\odot}$) from Pop III stars and PISNe that do not have mixed helium cores, preserving the layered elemental structure, have much flatter extinction curves in the UV arising from the absence of very small grains. The smallest grains experience the most destruction by thermal sputtering over the course of the reverse shock (e.g., Nath et al. 2008). Indeed the evolutionary phases of SNe and particularly the reverse shock have a profound impact on the grain properties and therefore their corresponding attenuation law (see Micelotta et al. 2018 for a thorough review). To characterize the processed properties of SNe dust, Bianchi & Schneider (2007) evolve a dust model of core collapse SNe ejecta through the reverse shock. The attenuation models of Bianchi & Schneider (2007) show a mild 2175Å bump and is more gray (i.e., flat) in the UV than MW and SMC-like laws as shown on Figure 1.

Markov et al. (2023, 2024) and Fisher et al. (2025) take a different approach by modeling the attenuation law directly whereby the parameters controlling its slope at different wavelengths as well as the 2175Å bump strength vary freely during fits. The mean attenuation law Markov et al. (2024) derive for galaxies with $6.3 < z_{\text{spec}} < 11.5$ is shown on Figure 1 and exhibits greater attenuation in the UV compared to a pure SNe dust law, but less attenuation relative to the SMC law. Markov et al. (2024) and Fisher et al. (2025) both note that this likely arises from grain reprocessing, possibly driven by SNe shocks preferentially destroying the small grains. Our approach in this work is complimentary to that of Markov et al. (2023, 2024) and Fisher et al. (2025). We test the limiting assumption of pure SNe dust which removes degeneracies with other stellar population synthesis properties that may otherwise change the UV slope. Both approaches are needed to test the nature of dust attenuation at very early cosmic times.

For the purposes of testing the impact of SNe dust attenuation laws on the *JWST* observations of $z > 6$ galaxies we adopt the empirical attenuation law of SNe 2012cu presented in Gao et al. (2020). As shown on Figure 1 the shape of A_{λ} for SNe 2012cu traces the median of the SNe dust models from Hirashita et al. (2005) and Bianchi & Schneider (2007) above $\sim 1500\text{\AA}$. Below this threshold the models exhibit steeper UV slopes, similar in shape to the SMC law but with > 2 mag less attenuation for fixed $A_{3000\text{\AA}}$ or A_V relative to SMC A_{λ} . Given their broadly similar shapes we prefer the empirical SNe dust laws.

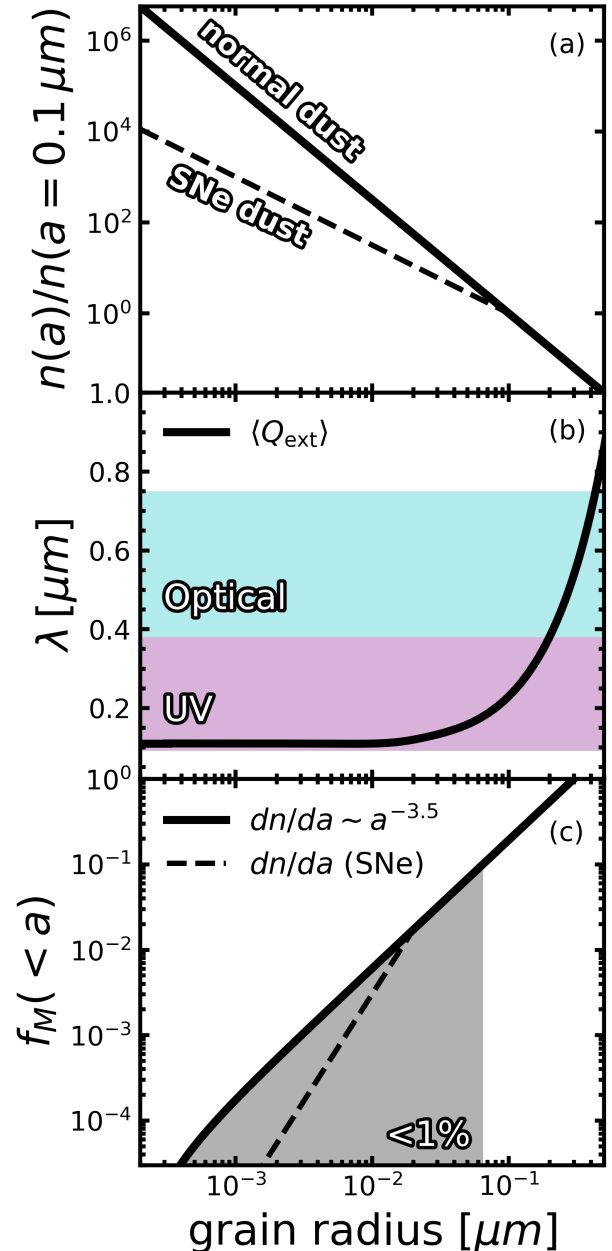


Figure 2. (a) Grain size distribution normalized at $0.1 \mu\text{m}$ for standard dust (solid) and SNe dust (dashed) with a break below $\approx 0.02 \mu\text{m}$. (b) The rest-frame wavelength corresponding to the average extinction efficiency Q_{ext} for a grain of size a , based on the *Astrodust* model (Draine & Hensley 2021; Hensley & Draine 2023). Below $a \approx 0.016 \mu\text{m}$ Q_{ext} converges to the Lyman limit which is also the wavelength limit of *Astrodust*. Grains with $a \lesssim 0.2 \mu\text{m}$ contribute to UV attenuation, but the total UV attenuation is dominated by very small grains with $a \lesssim 0.01 \mu\text{m}$ that are $\sim 10^4\times$ more numerous because of the steep power-law grain size distribution. (c) The fraction of mass in dust grains with size $< a$. In all cases 90% of the total dust mass is accounted for by grains with $a > 0.1 \mu\text{m}$ that contribute negligibly to the total UV attenuation.

2.1. The impact of attenuation laws on the inferred total dust mass

Dust grains responsible for attenuating UV light comprise a negligible fraction of the total dust mass. Therefore, the same quantity of dust can shape the observed UV spectrum of galaxies in very different ways depending on the underlying grain size distribution.

The variations between steep or shallow UV attenuation arise from small dust grains with grain radii $a < 0.1 \mu\text{m}$. Figure 2 (a) shows the grain size distribution for standard and SNe dust. Grains with sizes below $a \approx 0.01 \mu\text{m}$ are $\sim 10^4 \times$ more numerous than grains with $a = 0.1 \mu\text{m}$. Figure 2 (b) shows the wavelength corresponding to the average extinction efficiency Q_{ext}^1 for a grain of size a . Grains with $a \lesssim 0.1 \mu\text{m}$ all contribute to UV attenuation but the smallest grains ($a \lesssim 0.01 \mu\text{m}$) are dominant because they preferentially absorb at shorter wavelengths and are far more numerous. Assuming the standard power-law distribution in grain sizes $dn/da \sim a^{-3.5}$ (Mathis et al. 1977), the total mass of dust grains M_d with sizes between a_- and a_+ is

$$M_d \sim \int_{a_-}^{a_+} m(a)n(a) da \sim \int_{a_-}^{a_+} \frac{4}{3} \pi \bar{\delta}_g a^3 a^{-2.5} da \quad (1)$$

$$\sim \int_{a_-}^{a_+} \sqrt{a} da \propto [a^{3/2}]_{a_-}^{a_+}$$

where $\bar{\delta}_g$ is the mean grain density. Thus the fractional mass of grains of size $< a$ in the truncated range of $[a_-, a_+] = [2 \times 10^{-4} \mu\text{m}, 0.3 \mu\text{m}]$ is

$$f_M(< a) = \frac{a^{3/2} - a_-^{3/2}}{a_+^{3/2} - a_-^{3/2}} \quad (2)$$

as shown in Figure 2c. Based on the calculations of Nozawa et al. (2003), the size distribution of SNe dust has a characteristic break below $a_{\text{crit}} \approx 0.02 \mu\text{m}$ where $dn/da \sim a^{-2.5}$, reflective of the shift towards larger grain sizes on-average. In this regime we have $M_d(a) \propto a^{2.5}$ following the same approach.

Figure 2c shows the fractional mass in grains of size a between $2 \times 10^{-4} \mu\text{m}$ and $0.3 \mu\text{m}$. In both the standard power-law size distribution and for a SNe break below $0.02 \mu\text{m}$, grains of size $a > 0.1 \mu\text{m}$ contribute $> 90\%$ to the total dust mass. The grains most responsible for UV absorption have $a \approx 0.01 \mu\text{m}$ or smaller and account for $< 1\%$ of the total dust mass. As a result, the use of SNe attenuation laws will not lead to an observed shift

on M_d , and total dust masses will agree with what is otherwise allowed by other attenuation laws.

3. HIGH-REDSHIFT GALAXY OBSERVATIONS

Prior to *JWST* the number of spectroscopically-confirmed galaxies having redshifts greater than 7 was fewer than 20 (e.g., Ouchi et al. 2020). Deep *JWST* imaging surveys and their spectroscopic follow-up programs have now revealed hundreds of galaxies with confirmed redshifts up to $z \sim 14$ (see Stark et al. 2025 for a review), thus providing excellent statistical samples to begin critically revising our assumptions about galaxies in the very early Universe.

Given that dust attenuation laws vary more significantly in the UV, the assumption of SNe dust attenuation is likely to have significant impact on the interpretation of UV continuum slopes (β), and total UV magnitudes (M_{UV}). The relatively shallower SNe dust attenuation laws may also allow greater values of A_V while preserving the observed UV spectral shape relative to SMC laws, which can impact the inferred total stellar mass. To build a robust sample for testing the impacts of SNe dust on these properties we select galaxies from the *JWST* Advanced Deep Extragalactic Survey (JADES, Eisenstein et al. 2023a, <https://doi.org/10.17909/8tdj-8n28>). We take photometry in NIRCcam medium and broad bands from Eisenstein et al. (2023b) based on the maps of Rieke et al. (2023). We also adopt spectroscopic redshifts based on NIRSpec/MSA spectroscopy from JADES (Bunker et al. 2024; D'Eugenio et al. 2024), the complementary NIRCcam/grism spectra from the First Reionization Epoch Spectroscopically Complete Observations survey (FRESCO, Oesch et al. 2023), and further NIRCcam imaging from the *JWST* Extragalactic Medium-band Survey (JEMS, Williams et al. 2023, <https://doi.org/10.17909/fsc4-dt61>). These data cover the GOODS-North and GOODS-South extragalactic legacy fields with ancillary multi-wavelength imaging from ground and space-based telescopes like *HST*. These galaxies are broadly representative of the average galaxies – in mass, UV color, and luminosity – of what has been observed to date with *JWST* with no reason to suspect a bias in dust characteristics.

From the JADES public catalog (Eisenstein et al. 2023b) we select all objects with spectroscopic redshifts $z \geq 6$ derived from at least one emission line in the medium-resolution grating, and/or two or more MSA prism lines. This yields a high-fidelity sample of 138 galaxies, with 82 (60%) having $6 < z_{\text{spec}} < 7$, 35 (25%) having $7 < z_{\text{spec}} < 8$, and 19 (14%) having $8 < z_{\text{spec}} < 10$. Two sources have $z > 10$. We adopt Kron aperture photometry PSF-matched to the

¹ For this calculation we adopt the tabulated extinction efficiencies of the *Astrodust* model as described in Hensley & Draine (2023) and Draine & Hensley (2021).

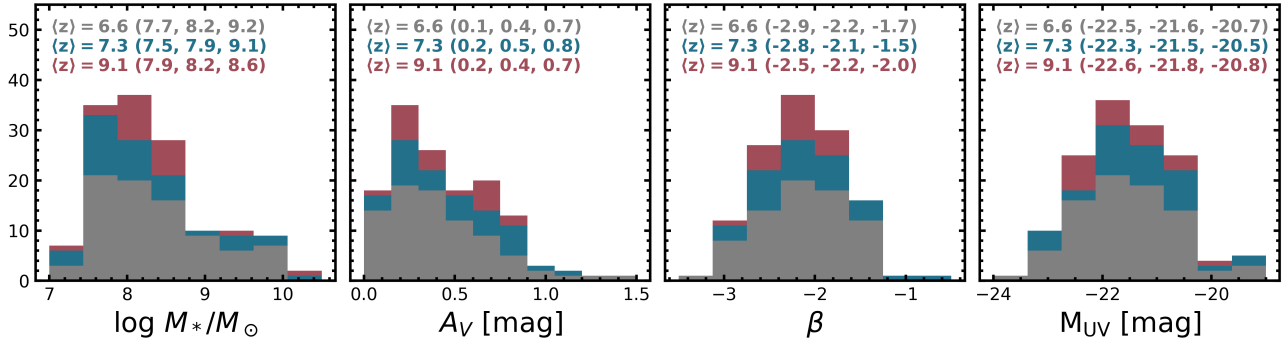


Figure 3. Stacked histograms of stellar mass, A_V , UV slope β , and total UV magnitude M_{UV} for our sample sub-divided into three redshift bins: $z < 7$ with mean $z = 6.6$ (black), $7 < z < 8$ with mean $z = 7.3$ (blue), and $z > 8$ with mean $z = 9.1$ (red). We report the 16th, 50th, and 84th percentiles in each redshift bin at the top of each panel.

NIRCam/F444W band following the convention of [Topping et al. \(2024\)](#) who also fit and analyze the UV slopes of JADES galaxies, but under the assumption of an SMC-like attenuation law. In this manner we collect PSF-matched photometry in the following NIRCam wide bands: F090W, F115W, F150W, F200W, F277W, F356W, and F444W as well as the medium band filters F182M, F210M, F335M, F410M, F430M, F460M, and F480M. We supplement these with PSF-matched photometry from *HST* also available from the JADES catalog in F435W, F606W, F814W, F850LP, F105W, F125W, F140W, and F160W.

We re-measure empirical UV slopes (β) following [Topping et al. \(2024\)](#) by fitting $f_\lambda \sim \lambda^{-\beta}$ to the F115W, F150W, and F200W filters for $5.4 < z_{\text{spec}} < 7.4$, F150W, F200W, and F277W for $7.4 < z_{\text{spec}} < 9.8$ and F200W, F277W, and F356W for $z_{\text{spec}} > 9.8$. To perform this fit we use the non-linear least-squares minimization algorithm as implemented in `lmfit` ([Newville et al. 2016](#)), which propagates the photometric uncertainties into the final errors on β . Our measured UV slopes are fully consistent with [Topping et al. \(2024\)](#) which is expected given the sample overlap.

4. SED FITTING WITH SUPERNOVA DUST

We fit the observed spectral energy distributions (SEDs) of our sample using BAGPIPES ([Carnall et al. 2018](#)) powered by `Nautilus` ([Lange 2023](#)), the latter of which implements a neural network approach to Bayesian posterior estimation. For a full description of BAGPIPES see [Carnall et al. \(2018\)](#). We adopt the standard assumptions of BAGPIPES as described therein. For each target we perform two runs with otherwise identical priors (see below) but with different attenuation laws. For the SNe dust model we adopt the empirical attenuation for SNe 2012cu from [Gao et al. \(2020\)](#). For the SMC model we adopt the standard SMC attenuation

law ([Gordon et al. 2003](#)) as implemented in the default BAGPIPES configuration ([Carnall et al. 2018](#)).

When fitting each target we fix the model redshift to the observed spectroscopic redshift. We include a nebular component with a radiation field density allowed to vary between $\log U \in (-4, 0)$ to cover the range of values observed in galaxies at $z > 6$ (e.g., [Tang et al. 2023](#)). We set an upper bound on the total stellar mass of $10^{11} M_\odot$ which in practice is never reached, and we let the metallicity vary between $10^{-4} Z_\odot$ and Z_\odot . We let A_V vary between 0 – 2. For each free parameter we assume uniform priors which are logarithmic for stellar mass, metallicity and nebular radiation density and are linear otherwise.

The choice of star-formation history can impact the final derived parameters. In this work we adopt the non-parametric model of [Leja et al. \(2019\)](#) which enforces a continuity prior between prescribed bins of variable SFR. We follow the parameter choices of [Markov et al. \(2023, 2024\)](#) who fit similar galaxies as those in our sample but with the intent of inferring the attenuation law as opposed to assuming its shape. We adopt $N = 7$ logarithmically spaced bins between the age of the Universe at each galaxy’s redshift out to a look-back time of $z = 20$. The parameter posteriors are generally insensitive to the number of bins for $N = 4 - 14$ ([Leja et al. 2019](#)). We measure the posterior distribution in observed M_{UV} by integrating the posterior SEDs convolved with a top hat filter between 1450Å and 1550Å.

We are most interested in the impact of SNe dust on the UV slope, the total UV luminosity, A_V , and the total stellar mass. These are well-constrained by the JADES filters that can recover the underlying continuum shape as well as the contamination in broad bands by strong emission lines thanks to the medium band coverage and sensitivity. Indeed [Yanagisawa et al. \(2024\)](#) find derived properties from NIRCam photometry and NIRSpect

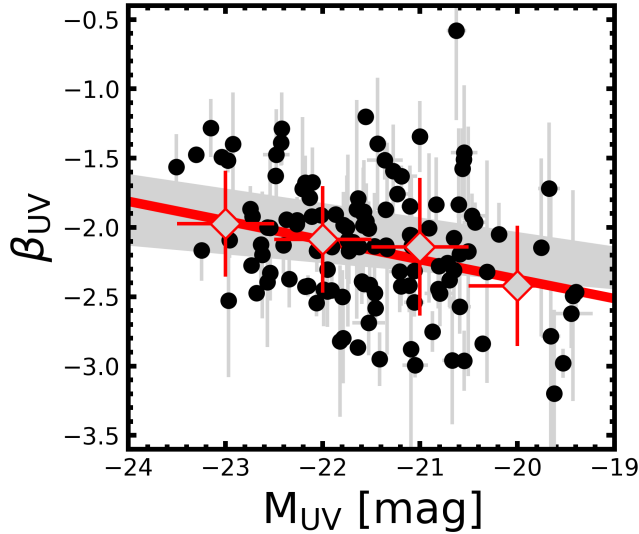


Figure 4. Empirical UV slopes β vs. the observed UV magnitudes taken from the best-fit models (black circles). The red diamonds show the weighted-average of β in bins of $\Delta M_{\text{UV}} = 2$. The grey region encases the trends from Topping et al. (2024) for sources with $z \sim 6 - 9$. The red line shows a linear fit to the binned average. Our results are generally consistent with the $\beta - M_{\text{UV}}$ trends of prior studies even with different dust prescriptions.

be consistent within the errors. Thus fitting only the photometry to back out the aforementioned quantities is well-motivated. BAGPIPES is capable of fitting to the available spectroscopy (Carnall et al. 2019) and implements a wavelength-dependent slit-loss correction polynomial that in principle is a function of the target’s morphology and the slit placement. This correction term can contribute to the models’ rest-frame continuum UV shape, which is also impacted by the star-formation history and dust attenuation. For this reason we choose to fit only the photometry, and leave fitting the joint photometry and spectra to future work.

5. RESULTS

5.1. Consistency with prior works

Figure 3 shows histograms for quantities derived from our observations and spectral energy distribution modeling. We measure stellar masses between $10^7 M_{\odot}$ and $10^{10} M_{\odot}$ with $A_V \in (0, 1.5)$ but most of the sample exhibit $A_V < 1$ which is within the range of prior works fitting for the attenuation in $z > 6$ galaxies using *JWST*/NIRCam and/or *JWST*/NIRSpec data (Markov et al. 2023, 2024; Langeroodi et al. 2024; Fisher et al. 2025). We measure UV slopes between $-3 < \beta < -1$, typical of other studies (Topping et al. 2024; Austin et al. 2024; Cullen et al. 2024; Morales et al. 2024), which is

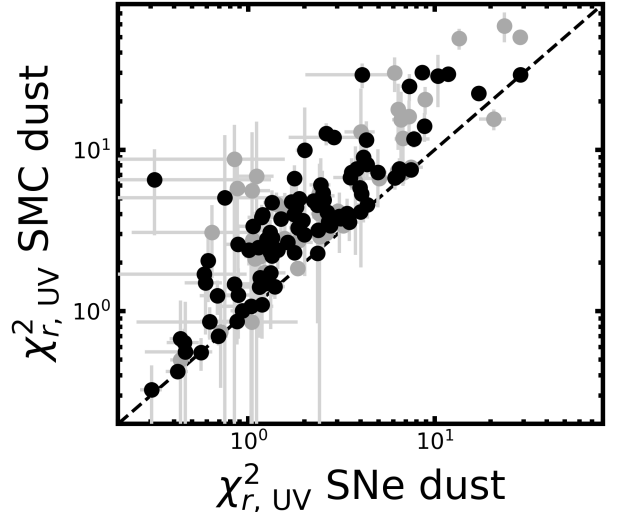


Figure 5. Reduced- χ^2 from models fits using SNe vs. SMC dust attenuation calculated in the rest-frame UV. The 1-to-1 relation is shown with the dashed black line, and black (gray) circles have consistent (inconsistent) star-formation histories as defined in Section 5.2. SNe dust attenuation laws find better fits to the rest-frame UV data of $z = 6 - 12$ galaxies.

expected as these are measured direct from the data and do not depend on our SNe dust assumptions. We infer observed $M_{\text{UV}} \in (-24, -19)$ which is consistent with the range in UV luminosities reported in prior works that in some cases adopt different spectral energy distribution model assumptions (e.g., Bunker et al. 2023; Topping et al. 2024). As shown Figure 4, we are able to recover the anti-correlation between UV slope and observed UV luminosity found in prior works (e.g., Topping et al. 2024) that do not use SNe dust.

5.2. Comparison with SMC-like attenuation

As described in Section 4 we perform another set of BAGPIPES fits to the data with identical priors but adopting an SMC attenuation law. Formally the two fits yield similar likelihood distributions per source and over the full sample. This is largely a product of the models’ success in reproducing the redder NIRCam bands that have high signal-to-noise ratios, especially when strong emission lines dominate their flux densities. Figure 5 shows the reduced- χ^2 calculated only with photometry covering the rest-frame UV. Models using SNe dust attenuation yield better fits to the UV than those assuming SMC-like dust attenuation. As a result, the observed UV luminosities measured from the SNe dust fits are fainter by $0.23^{+0.18}_{-0.16}$ mag as shown in Figure 6.

When comparing the two model runs we want to control for variations in the preferred star-formation histories. To quantify this we calculate a χ^2 -like statistic

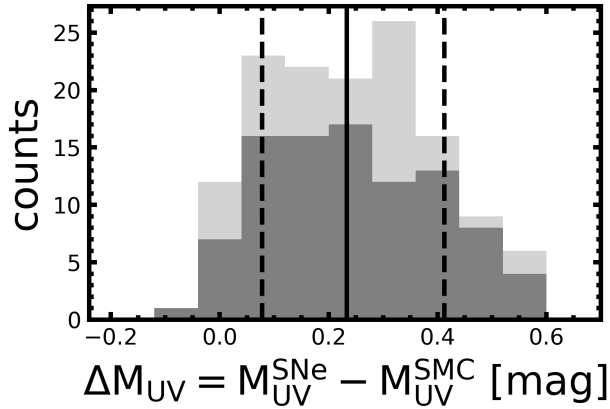


Figure 6. Stacked histogram showing the change in M_{UV} measured from the model SEDs assuming SNe vs. SMC dust attenuation. The dark (light) gray histogram corresponds to sources with convergent (divergent) star-formation histories between the two fitting assumptions. SNe dust attenuation leads to fainter observed M_{UV} by $0.23^{+0.18}_{-0.16}$ mag.

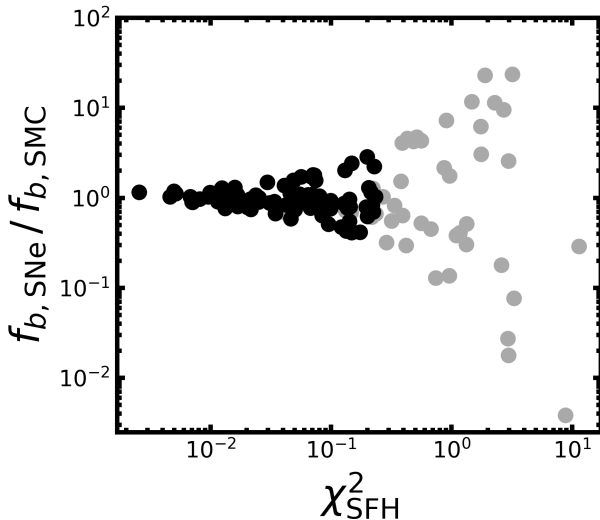


Figure 7. Star-formation history consistency between fits with SNe and SMC dust, using the 10 Myr burst fraction f_b and χ_{SFH}^2 as defined in Equation 3. We consider star-formation histories between these two runs to be consistent (black) when the burst fractions agree within 20% or $\chi_{\text{SFH}}^2 < 0.25$. 96/138 (70%) fits are consistent, and the remaining 30% prefer different star-formation histories when changing just the attenuation law.

from the star-formation histories. In BAGPIPES’ non-parametric implementation each age bin is assigned a $\Delta \log \text{SFR}_n \equiv \log \text{SFR}_n / \text{SFR}_{n+1}$ which is fit freely under a continuity prior (Leja et al. 2019). From these quantities output for both the SNe dust and SMC dust

fits we calculate

$$\chi_{\text{SFH}}^2 \equiv \sum_n [\Delta \log \text{SFR}_{n, \text{SNe}} - \Delta \log \text{SFR}_{n, \text{SMC}}]^2 \quad (3)$$

which captures the total difference between the two star-formation histories. The 16th, 50th and 84th percentiles on the square of χ_{SFH}^2 are 0.1, 0.3, and 0.9. We also calculate a burst fraction f_b defined as the fraction of star-formation within the most recent (10 Myr) age bin relative to the integrated star-formation history. Figure 7 compares these metrics across the sample. We define consistency as having $\chi_{\text{SFH}}^2 \leq 0.25$ dex or f_b within 20% of one-another. Approximately 70% of the fits have consistent star-formation histories between the SNe and SMC attenuation runs, and we find no significant bias against the remaining 30% in β , M_{UV} , A_V or stellar mass.

Figure 8 shows the relative change in A_V and stellar mass when assuming SNe vs. SMC dust attenuation. Relative to the SMC law, SNe dust attenuation yields higher values for A_V and for most of the sample correspondingly larger stellar masses. The 16th, 50th, and 84th percentiles for $\Delta A_V \equiv A_V^{\text{SNe}} - A_V^{\text{SMC}}$ and $\Delta \log M_* \equiv \log M_*^{\text{SNe}} / M_*^{\text{SMC}}$ are (0.07, 0.23, 0.46) and (-0.1, 0.1, 0.2) respectively. For the subset with consistent star-formation histories we find 16th, 50th, and 84th percentiles for $\Delta \log M_*$ of (0, 0.1, 0.3) dex and (0.1, 0.2, 0.5) mag for ΔA_V . The fits that yield consistent star-formation histories follow a relation characterized by $\Delta \log M_* / \Delta A_V = 0.6$. On-average, the stellar masses increase by ~ 0.1 dex when assuming SNe dust, comparable to the systematics found when varying more standard attenuation laws in lower redshift galaxies (Reddy et al. 2015; Salim et al. 2016), as well as parametric attenuation laws out to $z \sim 10$ (Markov et al. 2023, 2024; Fisher et al. 2025).

6. DISCUSSION

As discussed in Section 2.1 changes to A_λ at UV wavelengths are driven by very small dust grains that make up $< 1\%$ of the total dust mass. Nevertheless, we make a first-order estimate of the dust masses in our sample as a consistency check against grain formation models arising from SNe. Direct observations of cold dust continuum along the Rayleigh-Jeans tail are the most robust method of measuring the total mass of dust (Scoville et al. 2016, 2017). In place of such constraint we follow Casey et al. (2024) in estimating M_{dust} from A_V and the observed galaxy sizes. This method follows from the scaling relation between A_V and the dust mass sur-

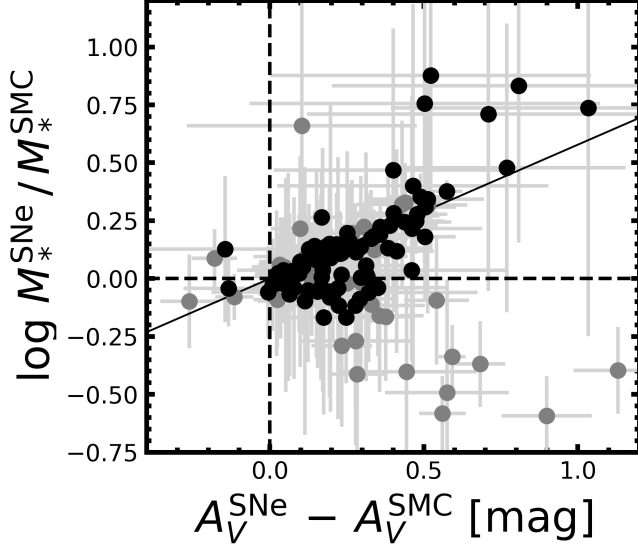


Figure 8. Change in stellar mass and A_V when assuming SNe vs. SMC dust attenuation. Solid black circles show fits that converge to similar star-formation histories under both attenuation law assumptions, whereas gray circles have divergent star-formation histories. The solid black line shows the best fit $\Delta \log M_* = 0.6\Delta A_V$ to fits with convergent star-formation histories. We find that assuming SNe dust leads to higher stellar mass estimates by up to ~ 0.8 dex and A_V by up to ~ 1 mag.

face density from [Draine et al. \(2014\)](#)². See [Casey et al. \(2024\)](#) for a detailed description. We use sizes as measured from F444W imaging to convert between the dust mass surface density and total dust mass. This method also allows us to test if the range in A_V , stellar mass and redshifts are plausibly consistent with dust formation mechanisms implicitly tied to our SNe attenuation assumption.

Figure 9 shows the resulting total dust-to-stellar mass predictions as a function of redshift. We overlay evolutionary models from SNe with and without reverse shock processing, as well as AGB stars from [Schneider & Maiolino \(2024\)](#) that all begin at a formation redshift of $z = 20$. We infer total dust-to-stellar mass ratios between 10^{-5} and 10^{-2} . Approximately 60% of the sample are consistent with SNe dust yields processed by reverse shocks. The remaining 40% are consistent with no shock processing; however, assuming the dust to be twice as compact as the F444W half-light radius would bring most of these into agreement with the rest of the sample. About 40% of the sample, including the two $z > 10$ sources, are consistent with AGB yields

² $A_V = 0.74 \times \Sigma_{\text{dust}} / 10^5 M_\odot \text{ kpc}^{-2}$ [mag]

but would need initial metallicities $0.1 < Z/Z_\odot < 1$ at $z = 20$ which could be difficult to achieve. The $z > 10$ galaxies exhibit dust-to-stellar mass ratios from our SNe dust fits fully consistent with SNe yields processed by reverse shocks with $Z/Z_\odot < 0.1$ at $z_{\text{form}} = 20$. Better constraints on both stellar mass and the total dust masses at these high-redshifts are needed to discriminate between the dust formation scenarios, and the effects of grain growth in the diffuse ISM may also play an important role ([Draine & Salpeter 1979](#); [Draine 2009](#); [Popping et al. 2017](#)). But as it stands the A_V -inferred dust masses coming from our SNe dust fitting are plausible given the current state of modeling dust yields at $z > 6$.

The decrease in observed M_{UV} we find when modeling dust attenuation with pure SNe dust laws might be important for interpreting $z > 8$ galaxies within a cosmological context. For instance, [Muñoz et al. \(2024\)](#) argue that current *JWST* observations predict far too many ionizing photons that would reionize the Universe by $z \sim 10$ in tension with the observed decline in neutral Hydrogen fraction between $z \sim 9 \rightarrow 6$. Essentially every parameter thought to regulate the ionizing photon rate is a function of M_{UV} , including the UV luminosity function and the production rate of ionizing photons per galaxy. Moreover, the ionizing photon escape fraction could be further impacted through the diverging properties of dust between the high- z galaxies driving reionization and the low- z counterparts where empirical relations are calibrated ([Chisholm et al. 2022](#)). Thus, the effects of a systematic decrease in observed M_{UV} due to SNe dust attenuation are non-linear and warrant more sophisticated modeling to better understand, which we leave to future work. But the trend is at least in the right direction in resolving the present tension by allowing for fewer ionizing photons with lower M_{UV} per galaxy.

Likewise, many works have found an over-abundance of bright sources compared to pre-*JWST* predictions (e.g., [Adams et al. 2023](#); [Harikane et al. 2023, 2024](#); [Finkelstein et al. 2023](#); [McLeod et al. 2024](#); [Whitler et al. 2025](#)). This has been interpreted as evidence for high star-formation efficiencies ([Dekel et al. 2023](#)), an absence of dust ([Ferrara et al. 2023](#); [Ferrara 2024](#); [Ferrara et al. 2024b](#); [Ziparo et al. 2023](#); [Fiore et al. 2023](#)), or bursty star-formation ([Mason et al. 2023](#); [Muñoz et al. 2023](#); [Sun et al. 2023](#)). SNe dust attenuation infers lower observed M_{UV} from the models which imply lower star-formation efficiencies; however, we also find that SNe dust attenuation finds larger stellar masses which could further exacerbate the inconsistencies with pre-*JWST* predictions. In either case, significant uncertainty re-

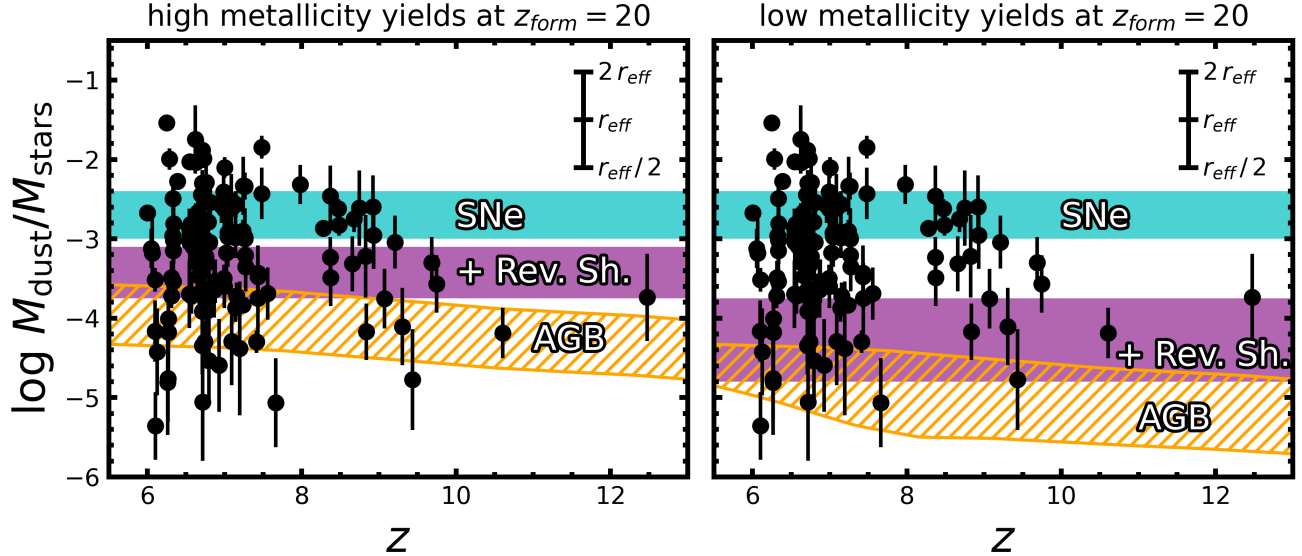


Figure 9. Total dust-to-stellar mass ratio as a function of redshift with dust masses predicted from A_V following Casey et al. (2024). We overlay the models of Schneider & Maiolino (2024) for SNe with (blue) and without (purple) reverse shock processing, as well as for AGB stars (orange hatched). The left and right panels show SNe and AGB yields when the initial metallicity at $z = 20$ is above or below $0.1Z_\odot$ respectively. In the upper right corner we illustrate the change in $\log M_{\text{dust}}/M_*$ that would arise from factors of two in radius. The predicted dust-to-stellar mass ratios are largely within the range of SNe yields with 60% favoring reverse shock processing and the remaining 40% requiring high yields with no destruction during the reverse shock. We emphasize that accurate dust masses are needed to validate the adoption of pure SNe dust attenuation laws; however, the dust-to-stellar mass ratios we infer from the modeled A_V are to first-order self-consistent with SNe yields assuming that the dust fully covers the extent of the rest-frame optical-emitting regions, and that the dust is optically thin.

mains in making reliable stellar mass measures for which understanding the dust attenuation law is just one of many important components.

7. CONCLUSION

We use pure supernovae dust attenuation laws to model the spectral energy distributions of $z_{\text{spec}} > 6$ galaxies. SNe dust has an intrinsically steeper grain size distribution characterized by fewer small ($a \sim 0.01 \mu\text{m}$) grains. This produces a much flatter UV attenuation curve than an SMC- or MW-like law. We adopt the attenuation law derived empirically for SN 2012cu by Gao et al. (2020) between $0.091 - 22.088 \mu\text{m}$ and implement it in BAGPIPES (Carnall et al. 2018), a spectral energy distribution modeling code. We then use BAGPIPES and the SNe dust attenuation law³ to model the *JWST*/NIRCam photometry from JADES (Eisenstein et al. 2023a) for 138 $z_{\text{spec}} > 6$ galaxies. Our main conclusions are:

1. A pure SNe dust attenuation law lets stellar population synthesis models find better fits to the rest-frame UV observation of $z \sim 6 - 12$ galaxies.

2. We recover a relation in UV slope and observed UV luminosity generally consistent with existing works that assume different dust attenuation laws.
3. We find systematically fainter observed UV luminosities by 0.23 mag on-average when assuming SNe dust because the models can find better fits with the gray SNe attenuation law.
4. When assuming SNe dust attenuation vs. SMC-like laws, total stellar masses increase by $0.1^{+0.2}_{-0.1}$ dex on-average, and A_V are higher by $0.3^{+0.2}_{-0.2}$ mag.
5. To first order SNe attenuation laws yield self-consistent total dust-to-stellar mass ratios given the formation timescales needed to build these dust reservoirs rapidly in the early Universe.

The wide-spread existence of significant dust reservoirs at $z > 6$ and the origins of that dust if present remains an open question. More work is needed to observationally confirm and characterize dust at early cosmic times, which can be achieved in the UV/optical through attenuation modeling or Balmer decrements, and also by observations at far-infrared/sub-mm wavelengths to observe dust in emission. Similarly, there is a strong need

³ <https://github.com/jed-mckinney/bagpipes-sne-dust>

for theoretical work and local observations to better constrain SNe dust properties and more generally the yields from all grain formation channels that may or may not be relevant. The impacts of dust assumptions are as important to the stellar mass and UV luminosity functions at these redshifts as variations in the underlying stellar models and star-formation histories.

JM thanks the UT Austin Cosmic Frontier Center community for the engaging discussions which motivated this work. JM acknowledges the invaluable labor of the maintenance and clerical staff at our institutions, whose contributions make our scientific discoveries a reality. JM thanks NASA and acknowledges support through the Hubble Fellowship Program, awarded by the Space Telescope Science Institute, which is operated by the Association of Universities for Research in Astronomy, Inc., for NASA, under contract NAS5-26555. OC and HA acknowledge support by the National Science Foundation Graduate Research Fellowship

under grant number DGE 2137420. JBM acknowledges support from NSF Grants AST-2307354 and AST-2408637, and by the NSF-Simons AI Institute for Cosmic Origins.

Authors from UT Austin acknowledge that UT is an institution that sits on indigenous land. The Tonkawa lived in central Texas, and the Comanche and Apache moved through this area. We pay our respects to all the American Indian and Indigenous Peoples and communities who have been or have become a part of these lands and territories in Texas. We are grateful to be able to live, work, collaborate, and learn on this piece of Turtle Island.

This work is based [in part] on observations made with the NASA/ESA/CSA James Webb Space Telescope. The data were obtained from the Mikulski Archive for Space Telescopes at the Space Telescope Science Institute, which is operated by the Association of Universities for Research in Astronomy, Inc., under NASA contract NAS 5-03127 for JWST. These observations are associated with programs GTO #1180, #1181, #1210, #1286, and GO #1895, #1963, and #3215.

REFERENCES

- Adams, N. J., Conselice, C. J., Ferreira, L., et al. 2023, *MNRAS*, 518, 4755, doi: [10.1093/mnras/stac3347](https://doi.org/10.1093/mnras/stac3347)
- Austin, D., Conselice, C. J., Adams, N. J., et al. 2024, arXiv e-prints, arXiv:2404.10751, doi: [10.48550/arXiv.2404.10751](https://doi.org/10.48550/arXiv.2404.10751)
- Bianchi, S., & Schneider, R. 2007, *MNRAS*, 378, 973, doi: [10.1111/j.1365-2966.2007.11829.x](https://doi.org/10.1111/j.1365-2966.2007.11829.x)
- Bunker, A. J., Saxena, A., Cameron, A. J., et al. 2023, *A&A*, 677, A88, doi: [10.1051/0004-6361/202346159](https://doi.org/10.1051/0004-6361/202346159)
- Bunker, A. J., Cameron, A. J., Curtis-Lake, E., et al. 2024, *A&A*, 690, A288, doi: [10.1051/0004-6361/202347094](https://doi.org/10.1051/0004-6361/202347094)
- Cardelli, J. A., Clayton, G. C., & Mathis, J. S. 1989, *ApJ*, 345, 245, doi: [10.1086/167900](https://doi.org/10.1086/167900)
- Carnall, A. C., McLure, R. J., Dunlop, J. S., & Davé, R. 2018, *MNRAS*, 480, 4379, doi: [10.1093/mnras/sty2169](https://doi.org/10.1093/mnras/sty2169)
- Carnall, A. C., McLure, R. J., Dunlop, J. S., et al. 2019, *MNRAS*, 490, 417, doi: [10.1093/mnras/stz2544](https://doi.org/10.1093/mnras/stz2544)
- Casey, C. M., Akins, H. B., Kokorev, V., et al. 2024, *ApJL*, 975, L4, doi: [10.3847/2041-8213/ad7ba7](https://doi.org/10.3847/2041-8213/ad7ba7)
- Chisholm, J., Saldana-Lopez, A., Flury, S., et al. 2022, *MNRAS*, 517, 5104, doi: [10.1093/mnras/stac2874](https://doi.org/10.1093/mnras/stac2874)
- Cullen, F., McLeod, D. J., McLure, R. J., et al. 2024, *MNRAS*, 531, 997, doi: [10.1093/mnras/stae1211](https://doi.org/10.1093/mnras/stae1211)
- Dekel, A., Sarkar, K. C., Birnboim, Y., Mandelker, N., & Li, Z. 2023, *MNRAS*, 523, 3201, doi: [10.1093/mnras/stad1557](https://doi.org/10.1093/mnras/stad1557)
- D'Eugenio, F., Cameron, A. J., Scholtz, J., et al. 2024, arXiv e-prints, arXiv:2404.06531, doi: [10.48550/arXiv.2404.06531](https://doi.org/10.48550/arXiv.2404.06531)
- Draine, B. T. 2009, in *Astronomical Society of the Pacific Conference Series*, Vol. 414, *Cosmic Dust - Near and Far*, ed. T. Henning, E. Grün, & J. Steinacker, 453, doi: [10.48550/arXiv.0903.1658](https://doi.org/10.48550/arXiv.0903.1658)
- Draine, B. T., & Hensley, B. S. 2021, *ApJ*, 909, 94, doi: [10.3847/1538-4357/abd6c6](https://doi.org/10.3847/1538-4357/abd6c6)
- Draine, B. T., & Salpeter, E. E. 1979, *ApJ*, 231, 438, doi: [10.1086/157206](https://doi.org/10.1086/157206)
- Draine, B. T., Aniano, G., Krause, O., et al. 2014, *ApJ*, 780, 172, doi: [10.1088/0004-637X/780/2/172](https://doi.org/10.1088/0004-637X/780/2/172)
- Eisenstein, D. J., Willott, C., Alberts, S., et al. 2023a, arXiv e-prints, arXiv:2306.02465, doi: [10.48550/arXiv.2306.02465](https://doi.org/10.48550/arXiv.2306.02465)
- Eisenstein, D. J., Johnson, B. D., Robertson, B., et al. 2023b, arXiv e-prints, arXiv:2310.12340, doi: [10.48550/arXiv.2310.12340](https://doi.org/10.48550/arXiv.2310.12340)
- Ferrara, A. 2024, *A&A*, 684, A207, doi: [10.1051/0004-6361/202348321](https://doi.org/10.1051/0004-6361/202348321)
- Ferrara, A., Carniani, S., di Mascia, F., et al. 2024a, arXiv e-prints, arXiv:2409.17223, doi: [10.48550/arXiv.2409.17223](https://doi.org/10.48550/arXiv.2409.17223)
- Ferrara, A., Pallottini, A., & Dayal, P. 2023, *MNRAS*, 522, 3986, doi: [10.1093/mnras/stad1095](https://doi.org/10.1093/mnras/stad1095)
- Ferrara, A., Pallottini, A., & Sommovigo, L. 2024b, arXiv e-prints, arXiv:2410.19042, doi: [10.48550/arXiv.2410.19042](https://doi.org/10.48550/arXiv.2410.19042)
- Ferrara, A., Sommovigo, L., Dayal, P., et al. 2022, *MNRAS*, 512, 58, doi: [10.1093/mnras/stac460](https://doi.org/10.1093/mnras/stac460)

- Finkelstein, S. L., Bagley, M. B., Ferguson, H. C., et al. 2023, *ApJL*, 946, L13, doi: [10.3847/2041-8213/acade4](https://doi.org/10.3847/2041-8213/acade4)
- Fiore, F., Ferrara, A., Bischetti, M., Feruglio, C., & Travascio, A. 2023, *ApJL*, 943, L27, doi: [10.3847/2041-8213/acb5f2](https://doi.org/10.3847/2041-8213/acb5f2)
- Fisher, R., Bowler, R. A. A., Stefanon, M., et al. 2025, arXiv e-prints, arXiv:2501.10541, doi: [10.48550/arXiv.2501.10541](https://doi.org/10.48550/arXiv.2501.10541)
- Gao, W., Zhao, R., Gao, J., Jiang, B., & Li, J. 2020, *Planet. Space Sci.*, 183, 104627, doi: [10.1016/j.pss.2018.12.010](https://doi.org/10.1016/j.pss.2018.12.010)
- Gordon, K. D., Clayton, G. C., Misselt, K. A., Landolt, A. U., & Wolff, M. J. 2003, *ApJ*, 594, 279, doi: [10.1086/376774](https://doi.org/10.1086/376774)
- Harikane, Y., Nakajima, K., Ouchi, M., et al. 2024, *ApJ*, 960, 56, doi: [10.3847/1538-4357/ad0b7e](https://doi.org/10.3847/1538-4357/ad0b7e)
- Harikane, Y., Ouchi, M., Oguri, M., et al. 2023, *ApJS*, 265, 5, doi: [10.3847/1538-4365/acaaa9](https://doi.org/10.3847/1538-4365/acaaa9)
- Hensley, B. S., & Draine, B. T. 2023, *ApJ*, 948, 55, doi: [10.3847/1538-4357/acc4c2](https://doi.org/10.3847/1538-4357/acc4c2)
- Hirashita, H., Nozawa, T., Kozasa, T., Ishii, T. T., & Takeuchi, T. T. 2005, *MNRAS*, 357, 1077, doi: [10.1111/j.1365-2966.2005.08730.x](https://doi.org/10.1111/j.1365-2966.2005.08730.x)
- Kawara, K., Hirashita, H., Nozawa, T., et al. 2011, *MNRAS*, 412, 1070, doi: [10.1111/j.1365-2966.2010.17960.x](https://doi.org/10.1111/j.1365-2966.2010.17960.x)
- Kroupa, P. 2001, *MNRAS*, 322, 231, doi: [10.1046/j.1365-8711.2001.04022.x](https://doi.org/10.1046/j.1365-8711.2001.04022.x)
- Lange, J. U. 2023, *Monthly Notices of the Royal Astronomical Society*, 525, 3181, doi: [10.1093/mnras/stad2441](https://doi.org/10.1093/mnras/stad2441)
- Langeroodi, D., Hjorth, J., Ferrara, A., & Gall, C. 2024, arXiv e-prints, arXiv:2410.14671, doi: [10.48550/arXiv.2410.14671](https://doi.org/10.48550/arXiv.2410.14671)
- Leja, J., Carnall, A. C., Johnson, B. D., Conroy, C., & Speagle, J. S. 2019, *ApJ*, 876, 3, doi: [10.3847/1538-4357/ab133c](https://doi.org/10.3847/1538-4357/ab133c)
- Markov, V., Gallerani, S., Ferrara, A., et al. 2024, *Nature Astronomy*, doi: [10.1038/s41550-024-02426-1](https://doi.org/10.1038/s41550-024-02426-1)
- Markov, V., Gallerani, S., Pallottini, A., et al. 2023, *A&A*, 679, A12, doi: [10.1051/0004-6361/202346723](https://doi.org/10.1051/0004-6361/202346723)
- Mason, C. A., Trenti, M., & Treu, T. 2023, *MNRAS*, 521, 497, doi: [10.1093/mnras/stad035](https://doi.org/10.1093/mnras/stad035)
- Mathis, J. S., Rumpl, W., & Nordsieck, K. H. 1977, *ApJ*, 217, 425, doi: [10.1086/155591](https://doi.org/10.1086/155591)
- McLeod, D. J., Donnan, C. T., McLure, R. J., et al. 2024, *MNRAS*, 527, 5004, doi: [10.1093/mnras/stad3471](https://doi.org/10.1093/mnras/stad3471)
- Micelotta, E. R., Matsuura, M., & Sarangi, A. 2018, *SSRv*, 214, 53, doi: [10.1007/s11214-018-0484-7](https://doi.org/10.1007/s11214-018-0484-7)
- Morales, A. M., Finkelstein, S. L., Leung, G. C. K., et al. 2024, *ApJL*, 964, L24, doi: [10.3847/2041-8213/ad2de4](https://doi.org/10.3847/2041-8213/ad2de4)
- Muñoz, J. B., Mirocha, J., Chisholm, J., Furlanetto, S. R., & Mason, C. 2024, *MNRAS*, 535, L37, doi: [10.1093/mnras/slaf086](https://doi.org/10.1093/mnras/slaf086)
- Muñoz, J. B., Mirocha, J., Furlanetto, S., & Sabti, N. 2023, *MNRAS*, 526, L47, doi: [10.1093/mnras/sladd115](https://doi.org/10.1093/mnras/sladd115)
- Nath, B. B., Laskar, T., & Shull, J. M. 2008, *ApJ*, 682, 1055, doi: [10.1086/589224](https://doi.org/10.1086/589224)
- Newville, M., Stensitzki, T., Allen, D. B., et al. 2016, *Lmfit: Non-Linear Least-Square Minimization and Curve-Fitting for Python*, *Astrophysics Source Code Library*, record ascl:1606.014
- Nozawa, T., Kozasa, T., Umeda, H., Maeda, K., & Nomoto, K. 2003, *ApJ*, 598, 785, doi: [10.1086/379011](https://doi.org/10.1086/379011)
- Oesch, P. A., Brammer, G., Naidu, R. P., et al. 2023, *Monthly Notices of the Royal Astronomical Society*, 525, 2864, doi: [10.1093/mnras/stad2411](https://doi.org/10.1093/mnras/stad2411)
- Oke, J. B. 1974, *ApJS*, 27, 21, doi: [10.1086/190287](https://doi.org/10.1086/190287)
- Ouchi, M., Ono, Y., & Shibuya, T. 2020, *ARA&A*, 58, 617, doi: [10.1146/annurev-astro-032620-021859](https://doi.org/10.1146/annurev-astro-032620-021859)
- Popping, G., Somerville, R. S., & Galametz, M. 2017, *MNRAS*, 471, 3152, doi: [10.1093/mnras/stx1545](https://doi.org/10.1093/mnras/stx1545)
- Reddy, N. A., Kriek, M., Shapley, A. E., et al. 2015, *ApJ*, 806, 259, doi: [10.1088/0004-637X/806/2/259](https://doi.org/10.1088/0004-637X/806/2/259)
- Rieke, M. J., Robertson, B., Tacchella, S., et al. 2023, *ApJS*, 269, 16, doi: [10.3847/1538-4365/acf44d](https://doi.org/10.3847/1538-4365/acf44d)
- Salim, S., & Narayanan, D. 2020, *ARA&A*, 58, 529, doi: [10.1146/annurev-astro-032620-021933](https://doi.org/10.1146/annurev-astro-032620-021933)
- Salim, S., Lee, J. C., Janowiecki, S., et al. 2016, *ApJS*, 227, 2, doi: [10.3847/0067-0049/227/1/2](https://doi.org/10.3847/0067-0049/227/1/2)
- Sarangi, A., Dwek, E., & Kazanas, D. 2019, *ApJ*, 885, 126, doi: [10.3847/1538-4357/ab46a9](https://doi.org/10.3847/1538-4357/ab46a9)
- Schneider, R., & Maiolino, R. 2024, *A&A Rv*, 32, 2, doi: [10.1007/s00159-024-00151-2](https://doi.org/10.1007/s00159-024-00151-2)
- Scoville, N., Sheth, K., Aussel, H., et al. 2016, *ApJ*, 820, 83, doi: [10.3847/0004-637X/820/2/83](https://doi.org/10.3847/0004-637X/820/2/83)
- Scoville, N., Lee, N., Vanden Bout, P., et al. 2017, *ApJ*, 837, 150, doi: [10.3847/1538-4357/aa61a0](https://doi.org/10.3847/1538-4357/aa61a0)
- Shimizu, T., Kawara, K., Sameshima, H., et al. 2011, *MNRAS*, 418, 625, doi: [10.1111/j.1365-2966.2011.19512.x](https://doi.org/10.1111/j.1365-2966.2011.19512.x)
- Stark, D. P., Topping, M. W., Endsley, R., & Tang, M. 2025, *ApJL*, 955, L35, doi: [10.3847/2041-8213/acf85a](https://doi.org/10.3847/2041-8213/acf85a)
- Sun, G., Faucher-Giguère, C.-A., Hayward, C. C., et al. 2023, *ApJL*, 955, L35, doi: [10.3847/2041-8213/acf85a](https://doi.org/10.3847/2041-8213/acf85a)
- Tamura, Y., Mawatari, K., Hashimoto, T., et al. 2019, *ApJ*, 874, 27, doi: [10.3847/1538-4357/ab0374](https://doi.org/10.3847/1538-4357/ab0374)
- Tang, M., Stark, D. P., Chen, Z., et al. 2023, *MNRAS*, 526, 1657, doi: [10.1093/mnras/stad2763](https://doi.org/10.1093/mnras/stad2763)
- Todini, P., & Ferrara, A. 2001, *MNRAS*, 325, 726, doi: [10.1046/j.1365-8711.2001.04486.x](https://doi.org/10.1046/j.1365-8711.2001.04486.x)

- Topping, M. W., Stark, D. P., Endsley, R., et al. 2024, MNRAS, 529, 4087, doi: [10.1093/mnras/stae800](https://doi.org/10.1093/mnras/stae800)
- Whitler, L., Stark, D. P., Topping, M. W., et al. 2025, arXiv e-prints, arXiv:2501.00984, doi: [10.48550/arXiv.2501.00984](https://doi.org/10.48550/arXiv.2501.00984)
- Williams, C. C., Tacchella, S., Maseda, M. V., et al. 2023, ApJS, 268, 64, doi: [10.3847/1538-4365/acf130](https://doi.org/10.3847/1538-4365/acf130)
- Witstok, J., Shivaee, I., Smit, R., et al. 2023, Nature, 621, 267, doi: [10.1038/s41586-023-06413-w](https://doi.org/10.1038/s41586-023-06413-w)
- Yanagisawa, H., Ouchi, M., Nakajima, K., et al. 2024, arXiv e-prints, arXiv:2411.19893, doi: [10.48550/arXiv.2411.19893](https://doi.org/10.48550/arXiv.2411.19893)
- Zavala, J. A., Casey, C. M., Manning, S. M., et al. 2021, ApJ, 909, 165, doi: [10.3847/1538-4357/abdb27](https://doi.org/10.3847/1538-4357/abdb27)
- Zavala, J. A., Castellano, M., Akins, H. B., et al. 2024, Nature Astronomy, doi: [10.1038/s41550-024-02397-3](https://doi.org/10.1038/s41550-024-02397-3)
- Ziparo, F., Ferrara, A., Sommovigo, L., & Kohandel, M. 2023, MNRAS, 520, 2445, doi: [10.1093/mnras/stad125](https://doi.org/10.1093/mnras/stad125)